

# A 3 × 6 arrayed CCD X-ray detector for continuous rotation method in macromolecular crystallography

Kazuki Ito,<sup>a\*‡</sup> Yurii Gaponov,<sup>b</sup> Noriyoshi Sakabe<sup>c</sup> and Yoshiyuki Amemiya<sup>d</sup>Received 28 July 2006  
Accepted 19 October 2006

<sup>a</sup>Institute of Materials Science, University of Tsukuba, 1-1-1 Tennodai, Tsukuba, Ibaraki 305-8573, Japan, <sup>b</sup>Photon Factory, Institute of Materials Structure Science, KEK, 1-1 Oho, Tsukuba, Ibaraki 305-0801, Japan, <sup>c</sup>Foundation for Advancement of International Science (FAIS), PF/IMSS KEK, Tsukuba, Ibaraki 305-0801, Japan, and <sup>d</sup>Department of Advanced Materials Science, Graduate School of Frontier Sciences, The University of Tokyo, 5-1-5 Kashiwanoha, Kashiwa-shi, Chiba 277-8561, Japan. E-mail: kazuki@spring8.or.jp

A 3 × 6 arrayed charge-coupled device (CCD) X-ray detector has been developed for the continuous-rotation method in macromolecular crystallography at the Photon Factory. The detector has an area of 235.9 mm × 235.9 mm and a readout time of 1.9 s. The detector is made of a 3 × 6 array of identical modules, each module consisting of a fiber-optic taper (FOT), a CCD sensor and a readout circuit. The outputs from 18 CCDs are read out in parallel and are then digitized by 16-bit analog-to-digital converters. The advantage of this detector over conventional FOT-coupled CCD detectors is the unique CCD readout scheme (frame transfer) which enables successive X-ray exposures to be recorded without interruption of the sample crystal rotation. A full data set of a lysozyme crystal was continuously collected within 360 s (180° rotation, 3 s/1.5° frame). The duty-cycle ratio of the X-ray exposure to the data collection time was almost 100%. The combination of this detector and synchrotron radiation is well suited to rapid and continuous data collection in macromolecular crystallography.

© 2007 International Union of Crystallography  
Printed in Singapore – all rights reserved**Keywords:** rapid data collection; continuous-rotation method; macromolecular crystallography; CCD X-ray detector.

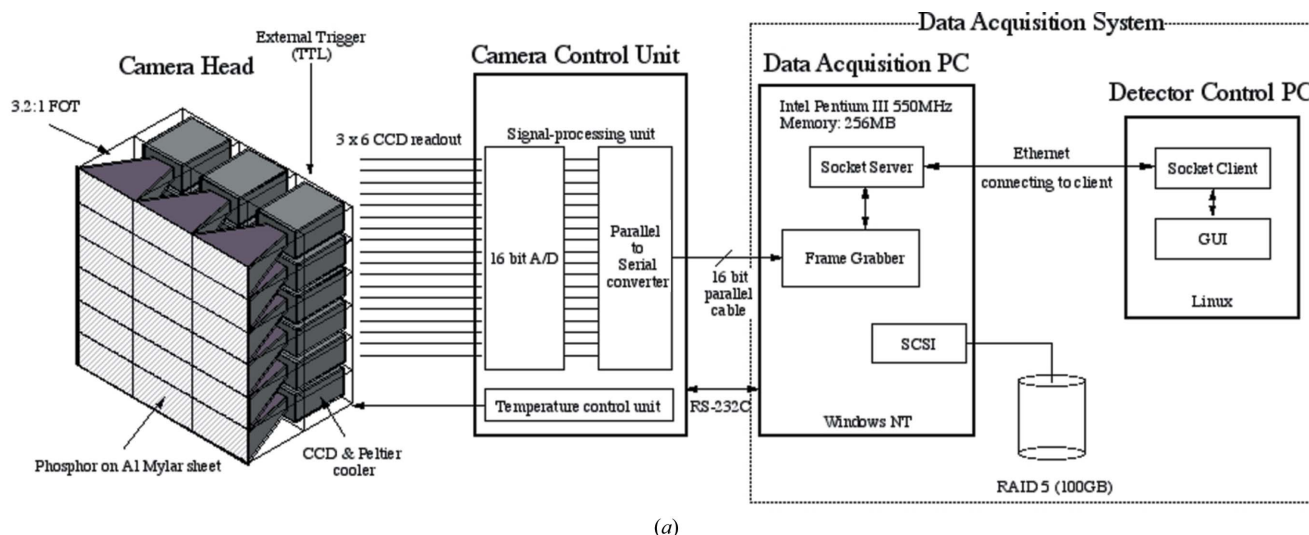
## 1. Introduction

In macromolecular crystallography the imaging plate (IP) has been widely used owing to the following excellent performance characteristics: no counting-rate limitation, wide dynamic range (six orders of magnitude), high detective quantum efficiency (DQE), and large active area size (over 300 mm × 300 mm) (Amemiya, 1995). However, a few minutes are required to read out the image and it also has to be mechanically exchanged from one exposure to another for the readout. Therefore, the overheads accompanied with the readout and exchange of IPs are usually much longer than the exposure time required to obtain a diffraction pattern with a synchrotron radiation source. These overheads can be shortened to less than 10 s using charge-coupled device (CCD) X-ray detectors because the readout time for CCDs is in the range of a few seconds. This is one of the main reasons why the CCD X-ray detectors attract attention.

Conventional CCD X-ray detectors use a demagnifying fiber-optic taper (FOT) to fit the small area of the CCD to the

larger active area required (Allinson, 1994; Tate *et al.*, 1995). In order to increase the active area, arrayed CCD X-ray detectors have been developed by several companies and research groups (Suzuki *et al.*, 1999; Phillips *et al.*, 2000; Area Detector Systems Corporation, <http://www.adsc-xray.com/>; Mar USA, <http://www.mar-usa.com/>; Oxford Instruments, <http://www.oxinst.com/>). These detectors use an external X-ray shutter and interrupt the crystal rotation during readout of the image data stored in the CCD. Moreover, with third-generation sources, typical exposure times required in macromolecular crystallography have been reduced from a few tens of seconds to a few seconds. Therefore, the overhead of a few seconds due to the CCD readout and interruption of the crystal rotation is no more negligible, and the duty-cycle ratio of the data collection becomes lower even with the CCD X-ray detectors. This is the reason why further reduction of the CCD readout time is required. However, this could only be marginally possible with the readout scheme of a full-frame transfer CCD, which is used in the conventional FOT-coupled CCD X-ray detector. To increase the duty-cycle ratio to close to 100% the 'continuous rotation' method was proposed (Ito *et al.*, 2000, 2004; Brönnimann *et al.*, 2003), coupled with fast framing detectors. In the case of a small-molecule crystal, the

‡ Present address: Structural Materials Science Laboratory, RIKEN Harima Institute/Spring-8 Center, 1-1-1 Kouto, Sayo-cho, Sayo-gun, Hyogo 679-5148, Japan.



(a)

continuous-rotation method was implemented using a micro-strip gas chamber (MSGC) (Ochi *et al.*, 2002) and  $\mu$ -PIC (Takeda *et al.*, 2005). However, the counting-rate capability and spatial resolution of the MSGC were not high enough to apply to macromolecular crystallography.

To achieve a 100% duty-cycle ratio of the data collection and high-counting-rate capability, we have developed a novel arrayed CCD X-ray detector on the basis of a unique readout scheme, called a 'frame-transfer' (FT), in collaboration with Hamamatsu Photonics (Ito *et al.*, 2004). At the beginning of this development a single-module FOT-coupled CCD X-ray detector was tested in order to determine the optimum demagnification ratio of the FOT and the phosphor material. Then a  $2 \times 2$  arrayed CCD X-ray detector was developed in order to test the data-acquisition system from the multi-modules and the FT-type CCD. Finally, we built a  $3 \times 6$  arrayed CCD X-ray detector (Ito *et al.*, 2000). We have also developed a correction method for the image distortion and non-uniform response of the arrayed CCD X-ray detector, which is based on the correction software (Ito *et al.*, 2005). The advantage of our detector over the conventional arrayed FOT-coupled CCD X-ray detectors is concerned with the unique readout scheme of the CCDs, which enables successive X-ray exposures to be recorded without any interruptions between them. In other words, neither the interruption of the rotation of the sample crystal nor the X-ray shutter for intermitted exposures is required during the data acquisition. This makes it possible to reduce the total length of the data collection time in macromolecular crystallography. In addition, the developed detector is very suitable for executing fine-slicing experiments. In this paper we will describe the design of the detector and its preliminary application to macromolecular crystallography with lysozyme and insulin.

## 2. Detector design

The  $3 \times 6$  arrayed CCD X-ray detector system consists of (i) a camera head, (ii) a camera control unit which includes a



(b)

**Figure 1**

(a) Schematic diagram of the  $3 \times 6$  arrayed CCD X-ray detector system. The detector system consists of a camera head, a camera control unit and a data-acquisition system including a data-acquisition PC and a detector-control PC. (b) Photograph of the camera head.

cooling system controller, and (iii) a data-acquisition system. A schematic of the  $3 \times 6$  arrayed CCD X-ray detector system is shown in Fig. 1(a).

### 2.1. Camera head

The camera head consists of a sheet of phosphor and a  $3 \times 6$  array of the identical detector modules. The phosphor [ $\text{Gd}_2\text{O}_2\text{S:Tb}$  (P43), Nichia Chemical, density  $15 \text{ mg cm}^{-2}$ ] is deposited onto an aluminized-Mylar sheet (thickness  $12 \mu\text{m}$ ,  $1000 \text{ \AA}$  Al deposited). The phosphor sheet can be easily fixed onto the detector by the atmospheric pressure. A photograph of the camera head of the  $3 \times 6$  arrayed CCD X-ray detector system is shown in Fig. 1(b). The camera head except the phosphor is evacuated by a small turbo molecular pump in order to reduce the heat conductance and to avoid condensation.

The detector module consists of a demagnifying FOT (Schott Fiber Optics), front-illuminated FT-type CCD (S7019-1009F, Hamamatsu Photonics) as an image sensor, a driver circuit and readout electronics of the CCD. The FOT has a demagnification ratio of 3.2:1 and a high X-ray resistance.

Each CCD that is bonded with a fiber-optic plate (FOP) is attached to a small end of the FOT. This method allows the mounted CCDs to be detached from the assembly easily, thus enabling the CCDs to be replaced by new ones. Incident X-rays are converted into visible light at the phosphor, and then are demagnified by the FOT, being introduced into each CCD. Each CCD chip has a load register and an impedance conversion buffer. The power dissipation of this circuit and heat production is negligibly small. The driver circuit and pre-amplifier for the CCD chip are located outside of the vacuum. These electronics are cooled by a fan and the power dissipation is 2 W for each CCD chip. Therefore, the total power dissipation concerned with the CCD drive and signal readout is less than 40 W. These driver circuits can also accept an external trigger pulse that starts the integration in the system.

The CCD chip has an area of 25 mm × 25 mm with 1024 × 1024 pixels (24 μm × 24 μm pixel size). The full-well capacity of the CCD chip is  $2.3 \times 10^5 \text{ e}^- \text{ pixel}^{-1}$ . The CCDs are cooled to 243 K with water-cooled Peltier devices in order to suppress the dark current. A 275 kHz pixel clock is used. The readout noise and dark current are  $12 \text{ e}^- \text{ r.m.s.}$  and  $0.5 \text{ e}^- \text{ s}^{-1} \text{ pixel}^{-1}$  at 243 K, respectively. The advantage of this detector over the conventional FOT-coupled CCD X-ray detectors is the unique CCD readout scheme. A schematic drawing of the FT-type CCD image sensor is shown in Fig. 2. Only the upper half area (1024 × 512 pixels) of each CCD is used as the active area, whereas the bottom half is used as a data storage area. The image data recorded in the active area are transferred to the data storage area within a time of 1.6 ms. The next image data can be recorded in the active area while the previous image data stored in the data storage area are transferred to a frame grabber in the data-acquisition system within a time of 1.9 s. This scheme enables successive X-ray diffraction patterns to be detected with a negligibly small intermission, that is, with an almost 100% duty-cycle ratio; neither an interruption of the crystal rotation nor an X-ray shutter for intermitted exposures are required during the data acquisition. This detector can also

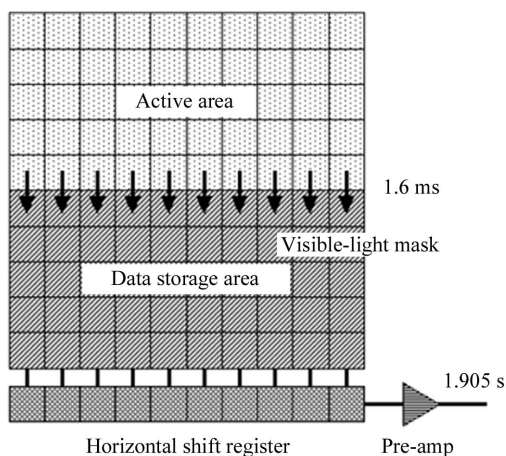


**Figure 2** Schematic drawing of a FT-type CCD image sensor. The image recorded in the ‘Active area’ can be transferred into the ‘Data storage area’ within 1.6 ms. The image data transferred into the ‘Data storage area’ are read out to the frame grabber in the data-acquisition PC within a time of 1.9 s.

simplify the data-acquisition system, because the crystal can be rotated continuously without interruption during the data acquisition.

## 2.2. Camera control unit

The camera control unit, produced by Hamamatsu Photonics, consists of three units: (i) a control and interface unit, (ii) a signal-processing unit and (iii) a temperature-control unit. The control unit has a serial interface (RS-232C) in order to receive the camera control commands from the data-acquisition personal computer (PC). The signal-processing unit has an array of 16-bit analog-to-digital converters (ADCs). The ADC gains can be selected low ( $4.05 \text{ e}^- \text{ ADU}^{-1}$ ), high ( $2.7 \text{ e}^- \text{ ADU}^{-1}$ ) and super-high ( $0.25 \text{ e}^- \text{ ADU}^{-1}$ ). The parallel outputs from the 18 ( $3 \times 6$ ) ADCs are converted to a 16-bit serial output in a multiplexer in the unit. The serialized output is transferred to the data-acquisition PC. The temperature-control unit drives 18 ( $3 \times 6$ ) Peltier devices, which have respective temperature sensors and stabilize the temperature at  $243 \pm 0.5 \text{ K}$  by PID control. Another function of the camera control unit is to inspect the status errors of the detector system: water circulation, water temperature and vacuum level. On detecting any of these status errors, the camera control unit turns off the power supply for the Peltier devices and indicates the LEDs on the status panel in front of the camera control unit. The status errors can be read out through the serial interface.

## 2.3. Data-acquisition system

The data-acquisition system consists of (i) a data-acquisition PC and (ii) a detector-control PC. The data-acquisition PC has a frame-grabber board and an external RAID storage that is connected through the SCSI interface. The serialized output from the camera control unit is transferred to the frame-grabber board (GRAPHIN IPM-8540D). The transferred data are rearranged into a two-dimensional image and stored in the RAID storage within 1.9 s. The stored image in the RAID storage can be remotely accessed over the TCP/IP socket through the Ethernet. This readout scheme can reduce the number of connection cables as well as frame-grabber boards and PCs, thereby reducing the development costs. The detector system is fully controlled through the network.

We modified the method of correcting the image distortion and non-uniform response for the arrayed CCD X-ray detector, which was originally developed for the beryllium-windowed X-ray image-intensifier coupled CCD X-ray detectors (Ito *et al.*, 2005). Moreover, the correction for the drift of the offset levels in CCDs was made by using optical black areas in the respective CCDs.

## 3. Data collection method

As described in §2.1, the exposure and readout periods can be fully overlapped, because the active and data storage area are physically isolated. Therefore this detector can continuously collect the image data without interruption of the crystal

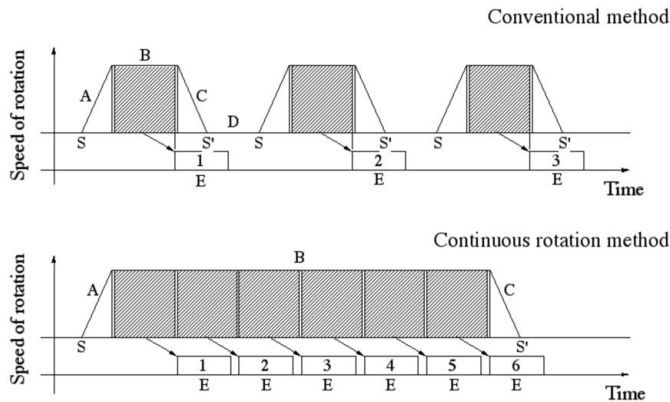


**Figure 3** Timing charts for the X-ray exposure and readout of the CCDs: conventional (upper) and continuous-rotation (lower) methods. The vertical and horizontal axes represent the speed of the crystal rotation and lap time, respectively. The numbers indicated in the charts correspond to the frame number. Letters denote the states of crystal rotation: A, acceleration; B, constant speed; C, deceleration; D, stop. S and S' denote the start and end time of the crystal rotation, respectively. The regions filled by oblique lines correspond to the exposure for the detector.

rotation when the exposure is longer than 1.9 s. It is a novel data collection method, a so-called 'continuous rotation' method (Ito *et al.*, 2000, 2004; Brönnimann *et al.*, 2003). On the other hand, a conventional FOT-coupled CCD X-ray detector, which uses a full-frame transfer readout, needs to close the X-ray shutter during the image readout because the photons impinging on the CCD during the readout are smeared in the direction of the charge transfer. Therefore, the exposure period cannot be overlapped with the readout period. In order to compare the continuous-rotation method with the conventional method, timing charts of the data collection are shown in Fig. 3. The data-collection duty-cycle ratio can be defined as the ratio of (exposure time):(exposure time + readout time) in a cycle. The advantage of our detector over the conventional method is maximized when the exposure time is the same as the readout time, that is 1.9 s.

The 3 × 6 arrayed CCD X-ray detector system can record an image during readout of the CCDs. The detector is still sensitive during the 1.6 ms time period of the image transfer from the active area to the data storage area in a CCD. The influence of a bright reflection in each pixel can theoretically happen, but so far this has not been observed.

#### 4. Performance characteristics

The performance characteristics of the 3 × 6 arrayed CCD X-ray detector were evaluated at BL-15A and BL-6B at the Photon Factory, IMSS/KEK. The parameters and performance characteristics of the detector are shown in Table 1.

##### 4.1. Conversion gain, noise and dynamic range

The conversion gain was measured using 8 keV X-rays. A square-shaped beam (1 mm × 1 mm) was used. The absolute intensity was measured using a germanium solid-state

**Table 1**

Detector parameters of the 3 × 6 arrayed CCD X-ray detector.

Active area size	235.9 mm × 235.9 mm
Pixel format	3072 pixels × 3072 pixels
Number of modules	18 (3 × 6)
Pixel size	76.8 μm × 76.8 μm (on the phosphor surface)
Phosphor	Gd <sub>2</sub> O <sub>2</sub> S:Tb (~15 mg cm <sup>-2</sup> )
Spatial resolution	100 μm (FWHM), 150 μm (FW at 10% maximum)
Readout time	1.9 s
Conversion gain	2.5 ± 0.5 e <sup>-</sup> per X-ray photon for 8 keV X-rays
Dynamic range	2 × 10 <sup>4</sup>
Full-well capacity	3 × 10 <sup>5</sup> e <sup>-</sup> pixel <sup>-1</sup>
Readout noise	12 e <sup>-</sup> r.m.s.
Dark current	0.5 e <sup>-</sup> s <sup>-1</sup> pixel <sup>-1</sup> at 243 K
Intensity resolution	16 bit
Exposure time	1.9–3600 s
External trigger input	Negative TTL
Image distortion	1%
Non-uniform response	2%

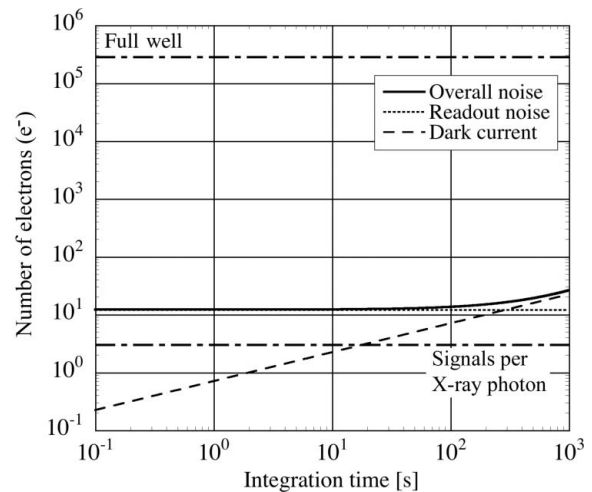


**Figure 4** Overall noise, readout noise and dark current of the 3 × 6 arrayed CCD X-ray detector are shown as a function of integration time. The units for the vertical axis are number of electrons. The full-well capacity and signals per X-ray photon are also indicated.

detector. The conversion gain shows that one X-ray photon creates 2.5 ± 0.5 electrons in the CCD chip. The overall noise of the detector,  $\sigma_t$ , can be written as follows,

$$\sigma_t = [\sigma_r^2 + \sigma_d^2 + (q^2/12)]^{1/2}, \quad (1)$$

where  $\sigma_r$  is the readout noise in the CCD chip,  $\sigma_d = (n_d t)^{1/2}$ , where  $n_d$  and  $t$  are the dark current in the CCD chip and the exposure time, respectively, and  $q$  is the number of electrons in an ADU. In (1) the third term in the parentheses denotes the quantization error of the ADC (Bennett, 1948); its contribution is usually negligible. The overall noise, readout noise and dark current of the 3 × 6 arrayed CCD X-ray detector are shown in Fig. 4 as a function of the integration time. The overall noise starts increasing at around an exposure time of 20 s owing to the increase in the dark current. In order for the signal level to exceed the overall noise, more than 4–5 X-ray photons of energy 8 keV are needed at an integration time of 20 s. The dynamic range is defined as the ratio of the full-well capacity of the CCD chip to the overall noise. The calculated

dynamic range of the  $3 \times 6$  arrayed CCD X-ray detector is  $2 \times 10^4$ .

### 4.2. Spatial resolution

The  $2 \times 2$  arrayed CCD X-ray detector, which was developed as a prototype of the  $3 \times 6$  arrayed CCD X-ray detector with identical specifications except for the number of modules, was used for the spatial resolution measurement. The spatial resolution was experimentally obtained by using a  $30 \mu\text{m}$ -diameter pinhole for 8 keV X-ray photons. The full widths at 50% and 10% of the maximum are  $100 \mu\text{m}$  and  $150 \mu\text{m}$ , respectively.

### 4.3. Image distortion and non-uniform response

The image distortion and non-uniform response of the detector were measured using visible light and 12.4 keV X-rays, respectively, on BL-6B at the Photon Factory. In general, a FOT-coupled CCD X-ray detector is affected by image distortion that is caused by the FOT. The grid mask, with 2.952 mm spacing, was printed onto a transparent sheet in black. The grid mask spacings are the same except for the region between modules in the vertical direction so as to sample the data points in detail (the spacing is 1.476 mm) at the module edge. The grid mask image recorded by the  $3 \times 6$  arrayed CCD X-ray detector is shown in Fig. 5(a). The degree of image distortion can be defined as  $|p_{\min} - p_{\max}|/p_{\text{ideal}}$ , where  $p_{\min}$ ,  $p_{\max}$  and  $p_{\text{ideal}}$  denote the maximum, minimum and ideal pixel sizes, respectively (Ito *et al.*, 2005). The histograms of the pixel size are calculated from the distances of observed grid mask spacings. The ideal pixel size of the  $3 \times 6$  arrayed CCD X-ray detector was determined to be  $72 \mu\text{m}$ , which minimized the global and local distortions in each module. In the case of a multi-module detector, the local distortion in each module was calculated and then merged with the global distortion with respect to the relative position between the modules. The image distortion calculated was  $|71.0 - 81.5|/72.0 = 14\%$  before the correction and  $|72.5 - 71.5|/72.0 = 1\%$  after the correction. The grid mask image after the image distortion correc-

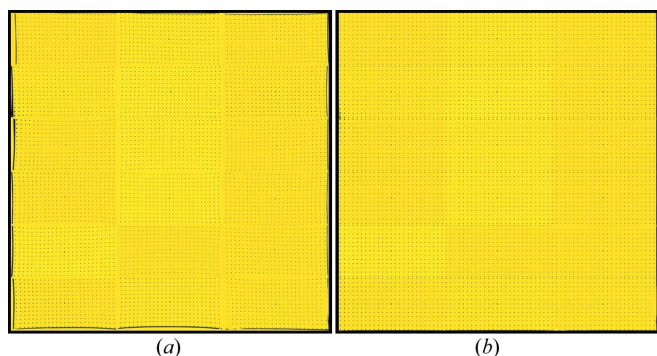


**Figure 5** Images recorded by the  $3 \times 6$  arrayed CCD X-ray detector with a grid mask which was placed in front of the detector. (a) Raw data and (b) with image distortion correction. Flood-field irradiation of the visible light was obtained with a light diffuser made of paper. The exposure time was 100 s and the detector gain setting of the detector was  $4.05 \text{ e}^- \text{ ADU}^{-1}$  (low gain).

tion is shown in Fig. 5(b). The dead area between the FOTs was evaluated to be about 0.3 mm (corresponding to  $\sim 4$ –5 pixels).

The  $3 \times 6$  arrayed CCD X-ray detector has a non-uniform response due to the following causes: (i) difference of CCD sensitivities and FOT transmissions, (ii) non-uniformity of the phosphor thickness and (iii) non-uniformity of the effective pixel size due to the image distortion. For the calibration of the non-uniform response, an imaging plate is placed at the input of this detector and is exposed to X-rays scattered by distilled water in the glass capillary at the sample position. Then the response curve of the imaging plate is used as a

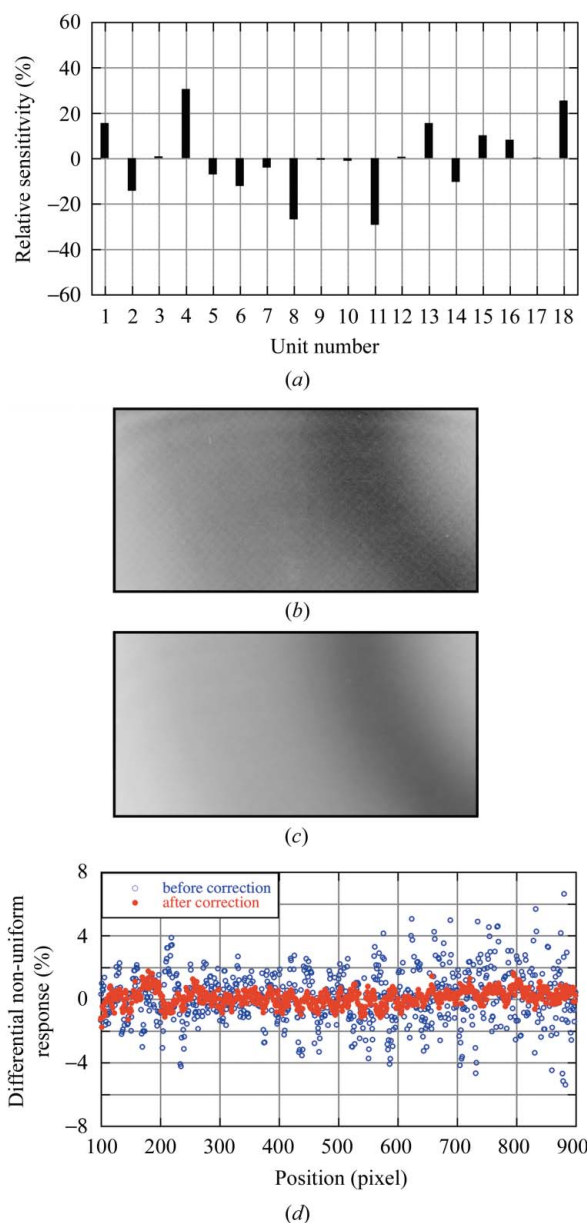


**Figure 6** (a) Non-uniform response (relative sensitivity) between detector modules. The flood-field image recorded by one of the detector modules (b) before and (c) after the correction. The flood-field was created by X-ray scattering from water in the capillary. (d) Differential non-uniform response along the horizontal direction of one detector module: before (open circles) and after (filled circles) the correction.

reference to be compared with that of this detector (Ito *et al.*, 2005). The non-uniform response can be evaluated by global and differential non-uniform responses. The global non-uniform response between detector modules is shown in Fig. 6(a). The scattering patterns from the distilled water in the glass capillary before and after the correction are shown in Figs. 6(b) and 6(c). The chicken wire due to the fiber bundle boundaries and phosphor grains due to deposition of the phosphor onto the aluminized Mylar sheet are clearly seen in Fig. 6(b). The differential non-uniform response was calculated in one of the detector modules along the horizontal direction shown in Fig. 6(d). The differential non-uniform response was  $\pm 4\%$  before the correction and it was reduced to  $\pm 1\%$  after the correction.

## 5. Experiments and results

The test experiments of the  $3 \times 6$  arrayed CCD X-ray detector were carried out on BL-6B at the Photon Factory, IMSS/KEK, by using two macromolecular crystals: tetragonal hen egg-white lysozyme and insulin. The sample-to-detector distance was 192 mm and the wavelength was 1.0 Å. The sample crystals were loaded into the glass capillary and then were mounted onto the goniometer using a piece of soft clay.

### 5.1. Lysozyme

Hen egg-white lysozyme is the standard sample for protein crystallography. A set of diffraction images was collected in 360 s (total  $180^\circ/120$  frames,  $1.5^\circ$  rotation/3 s exposure). The crystal was continuously rotated during the data collection. One of the sequence of diffraction images is shown in Fig. 7. The diffraction images were corrected for both image distortion and non-uniform response before processing. The diffraction images were indexed, integrated and processed statistically using the software *CrystalClear* (Rigaku, <http://www.rigaku.co.jp>). A summary is shown in Table 2. The *R*-merge and completeness were 14.163% in total (2.0 Å resolution) and 100.0%, respectively. The number of independent reflections was 8571 (2.0 Å resolution). Obtained *R*-merge values in each shell drastically increase with resolution above 2.7 Å; the cause is supposed to be the influence of low sensitivity of the detector.

### 5.2. Insulin

A set of diffraction data was collected within 368 s (total  $92^\circ/92$  frames,  $1.0^\circ$  rotation/4 s exposure). The crystal was continuously rotated during the data collection. The data were

**Table 2**

Processing statistics of a data set of tetragonal hen egg-white lysozyme by resolution shell.

Lysozyme cell parameters:  $a = 78.8950$  (45) Å,  $b = 78.8950$  (45) Å,  $c = 38.0255$  (26) Å,  $\alpha = 90.0^\circ$ ,  $\beta = 90.0^\circ$ ,  $\gamma = 90.0^\circ$ .

Resolution (Å)	Number of independent reflections	Number of multi-observed reflections	<i>R</i> -merge (%)	Accumulative <i>R</i> -merge (%)	$\chi^2$	$\langle I/\sigma \rangle$	
–	4.31	958	11014	5.693	–	0.614	8.51
4.31	3.42	881	10510	5.788	5.739	0.299	5.84
3.42	2.99	868	10781	7.927	6.194	0.352	4.26
2.99	2.71	835	10625	15.432	7.093	0.616	3.21
2.71	2.52	859	10822	28.585	8.469	1.044	2.43
2.52	2.37	835	10480	44.351	9.865	1.211	1.85
2.37	2.25	832	10880	51.246	11.249	1.261	1.60
2.25	2.15	849	11182	63.456	12.467	1.153	1.22
2.15	2.07	825	10828	67.490	13.496	1.012	1.04
2.07	2.00	829	9626	64.027	14.163	0.758	0.89
Total		8571	106748	14.163	14.163	0.836	3.94

**Table 3**

Processing statistics of a data set of insulin by resolution shell.

Insulin cell parameters:  $a = 82.5463$  (78) Å,  $b = 82.5463$  Å,  $c = 34.1270$  (49) Å,  $\alpha = 90.0^\circ$ ,  $\beta = 90.0^\circ$ ,  $\gamma = 120.0^\circ$ .

Resolution (Å)	Number of independent reflections	Number of multi-observed reflections	<i>R</i> -merge (%)	Accumulative <i>R</i> -merge (%)	$\chi^2$	$\langle I/\sigma \rangle$	
–	4.31	522	1663	5.304	–	3.214	18.70
4.31	3.42	534	1637	5.268	5.288	1.073	13.05
3.42	2.99	543	1652	6.006	5.408	1.022	9.00
2.99	2.71	556	1659	7.823	5.630	0.859	6.57
2.71	2.52	552	1653	9.500	5.852	0.785	5.06
2.52	2.37	558	1630	11.283	6.064	0.704	4.04
2.37	2.25	562	1635	11.982	6.279	0.711	3.74
2.25	2.15	558	1620	17.089	6.550	0.851	3.00
2.15	2.07	557	1583	22.913	6.869	1.181	2.59
2.07	2.00	509	1408	38.389	7.207	1.461	1.94
Total		5862	16140	7.207	7.207	1.183	8.78

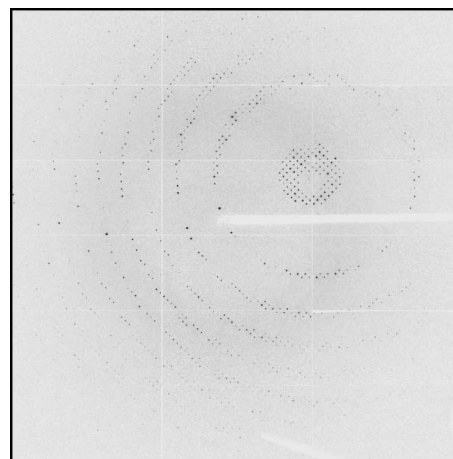


**Figure 7**

One of the diffraction images from the lysozyme crystal recorded by the  $3 \times 6$  arrayed CCD X-ray detector using the continuous-rotation method. The exposure time and crystal rotation speed of each frame were 3 s and  $0.5^\circ \text{ s}^{-1}$ , respectively.

processed as described in the previous section, and a summary is shown in Table 3. The data were corrected for both image distortion and non-uniform response. The *R*-merge and the

completeness were 7.207% in total (2.0 Å resolution) and 93.0%, respectively. The number of independent reflections was 5451 (2.0 Å resolution).

### 6. Conclusions

We have developed a  $3 \times 6$  arrayed CCD X-ray detector at the Photon Factory, IMSS/KEK, Japan. We have also characterized the detector performances, and its preliminary results have been demonstrated using macromolecular crystals (lysozyme and insulin) and synchrotron radiation on BL-6B, Photon Factory. An almost 100% duty-cycle ratio of the data collections using the continuous-rotation method was performed, with a total data collection time of 360 s for a  $180^\circ$  range with  $1.5^\circ$  per frame (lysozyme) and 368 s for a  $92^\circ$  range with  $1.0^\circ$  per frame (insulin). The advantage of this detector over conventional FOT-coupled CCD X-ray detectors is the unique CCD readout scheme that enables successive X-ray exposures to be recorded without interruption. In principle, the  $3 \times 6$  arrayed CCD X-ray detector can operate with an almost 100% duty-cycle ratio and perform the continuous-rotation method when the exposure time is more than 1.9 s. This feature is very suitable for rapid data collection in high-throughput macromolecular crystallography.

We are grateful for the financial support from the Photon Factory at the Institute of Materials Structural Science (IMSS) in the High Energy Accelerator Physics Organization (KEK), and the Japan Society for the Promotion of Science (JSPS,

Research for the Future Program, RFTF96R14501). We also thank Dr Higashi of Rigaku for beneficial discussions and data processing using *CrystalClear*. This work was performed under the approval of the Photon Factory Program Advisory Committee (Proposal Nos. 98G372 and 00G317).

### References

- Allinson, N. M. (1994). *J. Synchrotron Rad.* **1**, 54–62.  
Amemiya, Y. (1995). *J. Synchrotron Rad.* **2**, 13–21.  
Bennett, W. R. (1948). *Bell Syst. Tech. J.* **27**, 446–471.  
Brönnimann, C., Eikenberry, E. F., Horisberger, R., Hülsen, G., Schmitt, B., Schulze-Briese, C. & Tomizaki, T. (2003). *Nucl. Instrum. Methods, A* **510**, 24–28.  
Ito, K., Amemiya, Y., Higashi, T., Igarashi, N., Suzuki, M., Wakatsuki, S. & Sakabe, N. (2000). Photon Factory Activity Report, Part B, p. 292. Photon Factory, Tsukuba, Ibaraki, Japan.  
Ito, K., Gaponov, Y., Sakabe, N. & Amemiya, Y. (2004). *Proceedings of the 8th International Conference on Synchrotron Radiation Instrumentation (SRI2003)*, AIP Conference Proceedings Volume 705, pp. 227–230. New York: American Institute of Physics.  
Ito, K., Kamikubo, H., Yagi, N. & Amemiya, Y. (2005). *Jpn. J. Appl. Phys.* **44**, 8684–8691.  
Ochi, A., Tanimori, T., Nishi, Y., Nishi, Y., Nagayoshi, T., Ohashi, Y., Uekusa, H. & Toyokawa, H. (2002). *Nucl. Instrum. Methods, A* **477**, 48–54.  
Phillips, W. C., Stanton, M., Stewart, A., Qian, H., Ingersoll, C. & Sweet, R. M. (2000). *J. Appl. Cryst.* **33**, 243–251.  
Suzuki, M., Yamamoto, M., Kumasaka, T., Sato, K., Toyokawa, H., Aries, I. F., Jerram, P. A., Gullick, D. & Ueki, T. (1999). *J. Synchrotron Rad.* **6**, 6–18.  
Takeda, A., Uekusa, H., Kubo, H., Miuchi, K., Nagayoshi, T., Ohashi, Y., Okada, Y., Orito, R., Takada, A. & Tanimori, T. (2005). *J. Synchrotron Rad.* **12**, 820–825.  
Tate, M. W., Eikenberry, E. F., Barna, S. L., Wall, M. E., Lowrance, J. L. & Gruner, S. M. (1995). *J. Appl. Cryst.* **28**, 196–205.